Dynamics of oblate freely rising bodies

P. C. FERNANDES, P. ERN, F. RISSO and J. MAGNAUDET

Institut de Mécanique des Fluides de Toulouse, UMR CNRS/INP/UPS 5502,
Allée du Prof. C. Soula, 31400 Toulouse, France

Abstract. We have investigated the characteristics and the causes of the zigzag periodic motions followed by solid bodies rising freely under the effect of buoyancy in liquid otherwise at rest. The frequencies, amplitudes and relative phases of the body velocity and orientation have been determined for a large range of parameters. Thanks to the determination of the body kinematics and using the force and torque balances provided by the generalized Kirchhoff equations, we have analyzed the dynamics of the body periodic motion.

1. Introduction

We have investigated the zigzag periodic motion followed by a solid body rising freely under the effect of buoyancy in a liquid otherwise at rest. The central difficulty is tied to the intrinsic coupling between the fluid and body motions, the body displacement inducing a disturbance in the fluid which in turn imposes loads that govern the body motion. Also the governing equations and the interpretation of the hydrodynamic couplings between the various degrees of freedom become significantly more complex as soon as the body exhibits some geometrical anisotropy and starts rotating. Predicting the kinematics and the hydrodynamic loads on such freely-moving bodies as a function of the characteristic parameters of the fluid/body system is however of primary importance in many applications ranging from aerodynamics [13], meteorology [12], sedimentology [19] to biomechanics [20] and dispersed two-phase flows [14].

Freely rising or falling bodies in a fluid at rest can display various types of path and a number of investigations has thus been devoted to identify these paths and the range of parameters in which they occur. The canonical cases of a thin disk [21, 8] and that of a two-dimensional flat plate [1, 11] have been worked out in detail. In both cases, it turns out that, depending on the value of the control parameters, the motion can be rectilinear, planar time-periodic either without lateral drift or mean rotation (i.e. fluttering or zigzag) or with both of them (tumbling), quasi-periodic or even fully chaotic. Most of these regimes were also identified and analyzed numerically in the case of a solid sphere [10]. The kinematics and the dynamics of oblate gas bubbles as well as the motion induced in the liquid have also been investigated in detail experimentally [3, 18, 2] and by three-dimensional direct numerical simulations [16, 17].

The bodies considered here are short-length axisymmetric solid cylinders (Figure 1) of diameter d, thickness h and density ρ_s chosen very close to the density ρ_f of the liquid, $\rho_s/\rho_f \simeq 1$. The rising motion of the bodies was followed by two travelling

cameras; the time evolution of the position and orientation of the body was then determined by image processing. The characteristics of the body translation and rotation were investigated for aspect ratios, $2 < \chi = d/h < 20$, and Reynolds numbers, $100 < Re = V\,d/\nu < 300$, V being the vertical mean rise velocity of the body and ν the kinematic viscosity of the liquid. For some representative situations, the liquid motion induced by the body was characterized by either Particle Image Velocimetry (PIV) and dye visualization (Figure 2). We here summarize the main results of this study which are reported comprehensively in the papers [4]-[7].

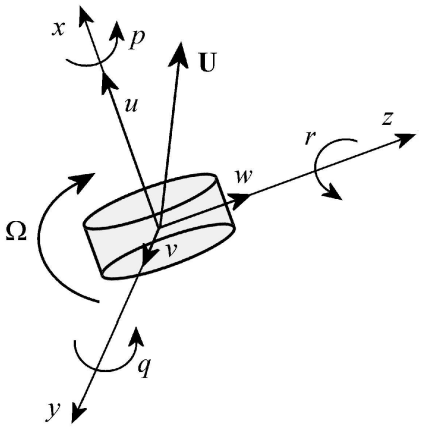

Figure 1. Sketch of the body with the rotating axes (x,y,z) and definition of the components of the velocity $\mathbf{U}$ and rotation rate $\mathbf{\Omega}$ of the body.

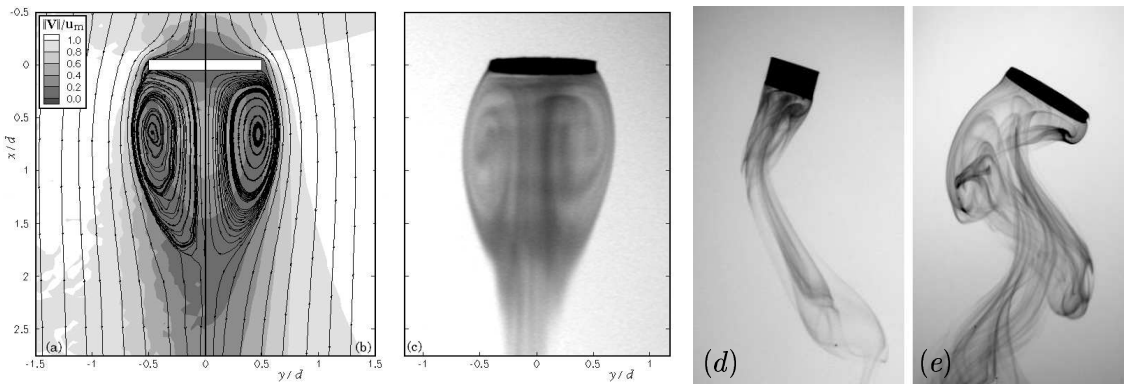

Figure 2. Velocity field for a steady case ($\chi = 10$, $Re = 100$): (a) freely rising body (rectilinear path; obtained by PIV), (b) fixed body (by DNS). Three dye-visualizations of the body wake: (c) rectilinear path ($\chi = 10$), (d) and (e) periodic path of a thick ($\chi = 2$) and a thin ($\chi = 10$) body, respectively.

2. Onset of the periodic path

The transition from the rectilinear rise to the oscillatory motion occurs for a critical Reynolds number Re_c that depends on the body aspect ratio χ. As shown

in Figure 3 (symbols), Re_c first decreases when χ increases, but then increases for $5 < \chi < 10$ and eventually becomes nearly independent of χ for thin bodies ($\chi > 10$). Since the periodic path is synchronized with the shedding of vortices, we have investigated the role of the wake instability on the body motion. We have therefore performed direct numerical simulations of the flow around fixed bodies of same shape and PIV measurements of the flow surrounding the freely-moving bodies. For all aspect ratios, the wake of the fixed body looses its axial symmetry above a critical Reynolds number Re_{c1} (plain line in Figure 3) and becomes unsteady at $Re_{c2} > Re_{c1}$ (dotted line). Both Re_{c1} and Re_{c2} decrease when the aspect ratio increases. For a Reynolds number Re smaller than Re_{c1}, the numerical result for the flow around a fixed body corresponds to the PIV measurements of the flow around the rectilinearly-rising body; in particular, the maximum of the reverse velocity V_t in the recirculation region, which characterizes the strength of wake effects, is the same. This velocity was shown to be an increasing function of the aspect ratio. Introducing the Reynolds number, $Re^* = V_t\, d/\nu$, which is related to Re through the empirical relation $\frac{0.62\chi}{1+\chi} Re$, the two wake bifurcations of the fixed body then correspond to constant values of Re^* whatever the aspect ratio, $Re^*_{c1} \simeq 72$ for the loss of axial symmetry and $Re^*_{c2} \simeq 78$ for the loss of stationarity. Figure 3 shows that for thick bodies ($\chi < 5$), the onset of path oscillation coincides with the first destabilization of the fixed body wake ($Re_c \approx Re_{c1}$), the wake instability causing a lift force and a torque able to induce the oscillatory motion. For thin bodies, on the contrary, the oscillatory motion appears at a Reynolds numbers higher than Re_{c2}. For $Re_{c2} < Re < Re_c$, PIV measurements have shown that the wake of the freely-rising thin body is still stationary. These results are presented in detail in ref. [7].

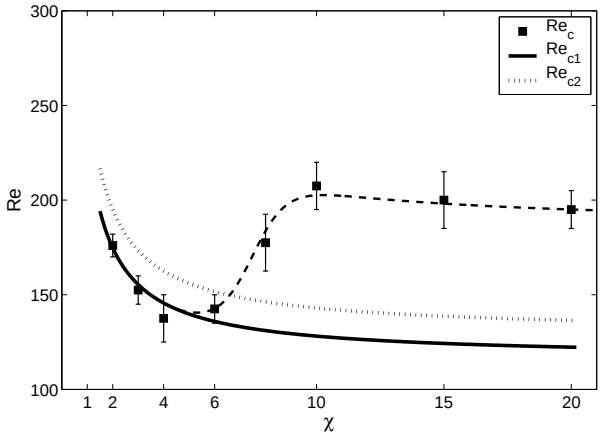

Figure 3. Onset of the oscillatory motion for a freely-rising body compared to the thresholds of the two successive wake instabilities of the same body when it is held fixed.

3. Characteristics of the oscillatory motion

For $Re > Re_c$, after a short transient following the release of the body from rest, the body exhibits a planar periodic motion, called zigzag or flutter. This motion is characterized by horizontal and vertical oscillations of constant amplitude superimposed to the body mean vertical rise, as well as oscillations of the body symmetry

axis about the vertical direction. In all cases, the orientation and the horizontal velocity oscillate at frequency f, whereas the vertical velocity oscillates at $2f$. We have shown that the body kinematics exhibit interesting properties in the system of axes sketched in Figure 1, where x is directed along the body symmetry axis, y and z along two perpendicular radial directions, (x,y) defining the plane of motion: the component of the body velocity parallel to its axis is constant along the path $u = \overline{u}$ and the oscillatory behaviour of the velocity is thus restricted to the transverse component v along the y direction. Figure 4 shows that the evolution with Re^* of the axial velocity $\overline{u}$ compared to the gravitational velocity $u_o = ((1 - \rho_s/\rho_f)\, g\, h)^{1/2}$ (g denoting gravity) can be conveniently modeled by equation (1). Similarly, scaling the transverse velocity v by fd, allowed us to gather all the results along a unique curve given by (2), the amplitude of which depends only on Re^*, as shown in Figure 5(left). The measurements of the amplitude of the body inclination θ (i.e. θ is the angle between the body symmetry axis x and the vertical) also gather along a master curve given by (3), the amplitude of which depends only on Re^* (Figure 5, right). The Strouhal number, $St = fd/V$, is approximately independent of Re but varies strongly with the aspect ratio, increasing from approximately 0.1 to 0.25 when χ varies from 2 to 10. This contrasts with the behaviour of the Strouhal number associated to the vortex shedding behind the bodies held fixed, since numerical simulations for Re just above Re_{c2} provided values nearly independent of the body aspect ratio: $St \approx 0.12$ for all χ. We have shown however that the Strouhal number St^* built with the gravitational velocity u_o follows a simple evolution in $\chi^{1/2}$ (equation (4), Figure 6, left). Though the body velocity and orientation oscillate at the same frequency, their phase difference depends strongly on the aspect ratio and is nearly independent of the Reynolds number: when χ varies from 2 to 10, the phase lag increases continuously from approximately 0 to 110° and then remains nearly constant for $\chi > 10$. The phase difference Φ_θ between the oscillations of θ and v also depends on the aspect ratio though it evolves in a shorter range, as can be seen in Figure 6(right). For further details, the reader is referred to ref. [5, 7].

$$\overline{u}/u_o \approx 1.35 - 3.5 \times 10^{-3}(Re^* - Re^*_{c1}), \tag{1}$$

$$v/(fd) \approx 9 \times 10^{-2}\pi(Re^* - Re^*_{c1})^{1/2} \sin(2\,\pi\, St^*\, t), \tag{2}$$

$$\theta \approx 5.8 \times 10^{-2}(Re^* - Re^*_{c1})^{1/2} \sin(2\,\pi\, St^*\, t + \Phi_\theta), \tag{3}$$

$$St^* = fd/u_o \approx 0.1\ \chi^{1/2}. \tag{4}$$

4. Forces and torques acting on the freely-moving body

The motion of a non-deformable body through an unbounded viscous fluid at rest at infinity is governed by the generalized Kirchhoff equations [9, 15], which express the linear and angular momentum balances for the complete fluid/body system. These equations are commonly written in the system of axes used previously with an origin fixed with respect to the observer and axes rotating with the body (Figure 1). For uniform fluid and body densities, they read

$$\left(\frac{\rho_s}{\chi\rho_f} + \mathrm{A}\right)\frac{du}{dt} - \left(\frac{\rho_s}{\chi\rho_f} + \mathrm{B}\right) v\, r = \mathrm{F}^x_\omega + \cos\theta \tag{5}$$

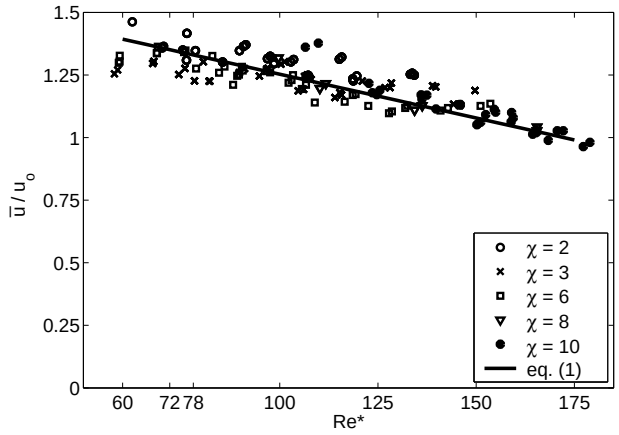

Figure 4. Mean axial velocity $\overline{u}$ normalized by u_o as a function of Re^* and χ. The fit corresponds to equation (1).

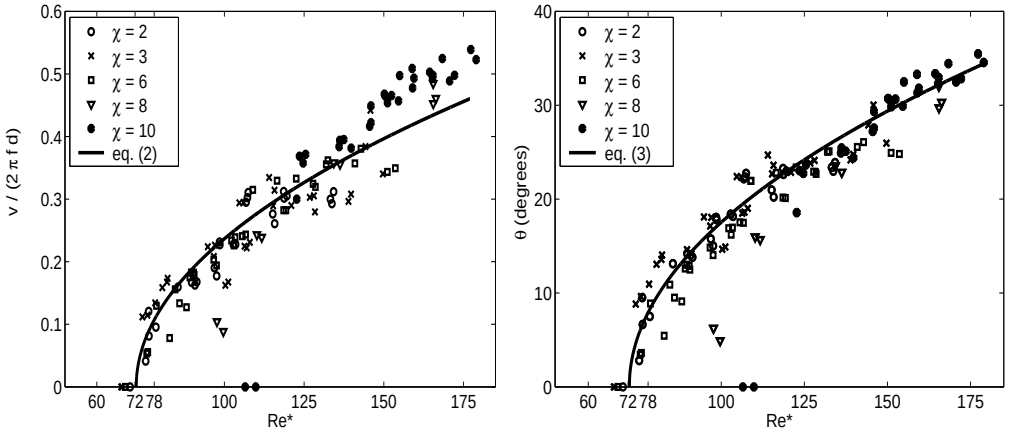

Figure 5. On the left : Evolution of the amplitude of the transverse velocity v scaled by $2\pi f d$ with Re^* and χ. On the right : Evolution of the amplitude of the body inclination θ as a function of Re^* and χ.

$$\left(\frac{\rho_s}{\chi\rho_f} + \mathrm{B}\right)\frac{dv}{dt} \;+\; \left(\frac{\rho_s}{\chi\rho_f} + \mathrm{A}\right) u\, r \quad = \quad \mathrm{F}_\omega^y \quad - \quad \sin\theta \tag{6}$$

$$\left(\frac{\rho_s}{\chi\rho_f}\mathrm{J}_2 + \mathrm{Q}\right)\frac{dr}{dt} \quad - \quad (\,\mathrm{A} - \mathrm{B}\,)\, u\, v \quad = \quad \Gamma_\omega^z \quad , \tag{7}$$

where $r = \frac{d\theta}{dt}$ is the body rotation rate about the z axis. Equations (5)–(7) are written in dimensionless form, using the scales $l_o = d$, $u_o = ((1 - \rho_s/\rho_f)\, g\, h)^{1/2}$, $t_o = l_o/u_o$, and $F_o = (\rho_f - \rho_s)\vartheta\, g$ for the length, velocity, time and force, respectively, ϑ being the body volume. The left-hand side of (5)–(7) contains the proper- and added-inertia force and torque, the coefficients A, B, J_2 and Q being known functions of the aspect ratio χ. The right-hand side of (5)–(7) contains the projections of the buoyancy force, which are harmonic functions of the inclination angle θ, and the

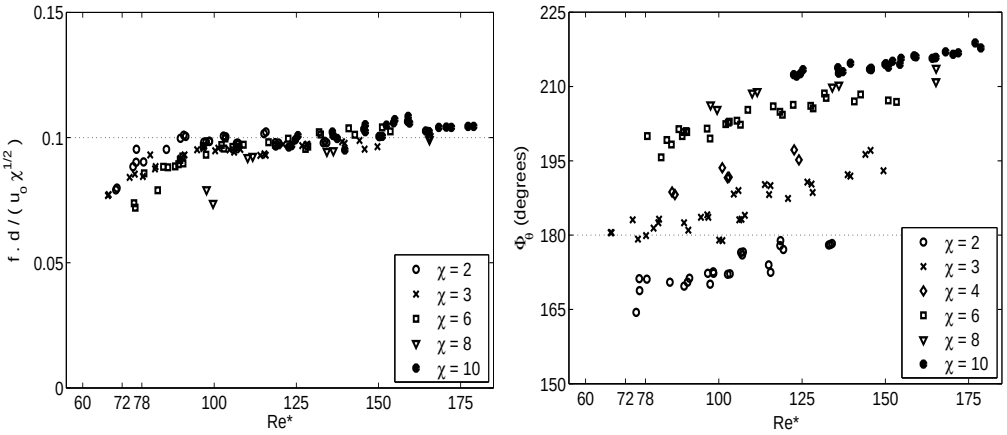

Figure 6. On the left : Scaling of the Strouhal number St^* with the aspect ratio. On the right : Evolution of the phase difference Φ_θ between the oscillations of the body orientation θ and of the transverse velocity v as a function of Re^* and χ.

components F_ω^x, F_ω^y and Γ_ω^z of the force and torque resulting from the vorticity produced at the body surface. In ref. [6], for the final periodic path on which all forces and torques evolve periodically, the inertia and buoyancy contributions were determined using the kinematic results of ref. [7] and the vortical loads were deduced from the balances (5)–(7). This led to the following conclusions regarding the main features of the body dynamics. The force balance in the axial direction is dominated by the steady components of drag and buoyancy, $\mathrm{F}_\omega^x \approx -1$, resulting in a constant axial velocity $u = \overline{u}$. In contrast the oscillatory contributions to the transverse force and torque balances are of the same order of magnitude as the mean drag. The transverse vortical force F_ω^y and the vortical torque Γ_ω^z exhibit harmonic oscillations at frequency St^*. Their amplitudes are plotted in Figure 7 as a function of Re^* and their phase difference (the force F_ω^y is in all cases ahead of the torque Γ_ω^z) is given by the dimensionless time delay t_d, displayed in Figure 9. Since $t_d \approx 0.8$ whatever Re and χ, the time delay between the transverse vortical force and the vortical torque is of the order of the characteristic time of the mean rise, i.e. $t_o = d/u_o$. This indicates that the problem is governed by two independent time scales. On the one hand, the body motion and the vortex shedding process have a periodicity of $f^{-1} \propto t_o \chi^{-1/2}$. On the other hand, the evolution of the vortical structures in the body wake is governed (at leading order) by the time scale t_o. In correspondance with the approximate expressions (1)–(4) provided for the body kinematics, the characteristics of the vortical loads can therefore be gathered in the following empirical expressions

$$\mathrm{F}_\omega^y \approx -\frac{1}{15}(Re^* - Re_{c1}^*)^{1/2} \sin(2\,\pi St^*\,(t + t_d)), \tag{8}$$

$$\Gamma_\omega^z \approx -\frac{\chi^{3/4}}{115}(Re^* - Re_{c1}^*)^{1/2} \sin(2\,\pi St^*\,t), \tag{9}$$

the expressions for the amplitudes corresponding to the curves drawn in Figure 7. The determination of the different terms of the Kirchhoff equations (5)–(7) is also instructive on how the loads combine to support the body periodic motion. Figure

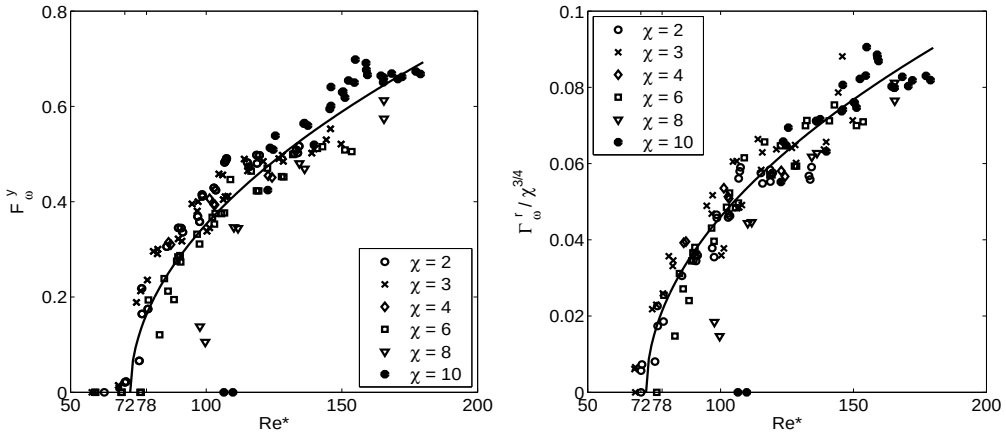

Figure 7. On the left : Evolution of the amplitude of the transverse vortical force F_ω^y with Re^* and χ. On the right : Evolution of the amplitude of the vortical torque Γ_ω^z with Re^* and χ.

8 presents for a thick ($\chi = 3$) and a thin ($\chi = 10$) body the time evolution of the predominant periodic loads governing the zigzag motion. Along the transverse direction, it turns out that the vortical force F_ω^y is mostly balanced by the sum of the inertia term proportional to the body rotation r, say F_{ur}^y, and the transverse component of buoyancy, say $F_g^y = \sin\theta$; the transverse linear acceleration of the body having a smaller contribution. Similarly, the inertia torque related to the angular acceleration of the body is negligible and the vortical torque Γ_ω^z is mostly balanced by the restoring added-mass torque associated with the transverse velocity component v. In particular, the stronger vortical torque observed for larger values of χ corresponds to a larger transverse velocity v, i.e. a larger angle between the symmetry axis and the instantaneous velocity of the body. It can therefore be noted that, on the one hand, the transverse vortical force F_ω^y is mainly balanced by two forces that depend on the body inclination and are $\pi/2$ out-of-phase, whereas the vortical torque is linked to the transverse velocity v. The chronology of the loads acting on the body can then be summarized as follows (the description is detailed in ref. [4] together with the evolution of the liquid motion obtained by PIV). Consider a body that is horizontal ($\theta = 0$) with a transverse vortical force acting on it, say $F_\omega^y < 0$. To balance this force, the body is rotating clockwise ($r < 0$), generating the inertia force F_{ur}^y. While the body rotates, a transverse component of the buoyancy force is generated, compensating partly for F_ω^y and allowing the body to decrease its rotation rate. Since the rotation also induces a rearrangement of the wake, the vortical force saturates and starts decreasing. This in turn allows the body to reach a maximum inclination, for which the buoyancy force and the transverse vortical force balance each other, which happens after a time period of $f^{-1}/4$. In parallel, the wake also generates a torque Γ_ω^z on the body, which is now negative, corresponding to a positive transverse velocity v, i.e. the velocity vector is to the left of the body axis. Since the maxima of the vortical force and torque are separated by a time period set by the mean rise motion t_o, when the body reaches its maximum inclination, the vortical torque either continues to grow ($\chi \geq 3$) or has just started decreasing ($\chi = 2$). Since the body axis starts now to rotate counter-clockwise, this results

in very different constraints on the velocity vector, leading to the different types of body motion described in ref. [5] : the thick body continues straight ahead and broadside on (v decreases in magnitude) whereas the velocity vector of the thin body has to rotate faster counter-clockwise (v increases in magnitude) so that the body leaves sideways.
The next step, for which a numerical approach might be better suited, could be to determine quantitatively the rate at which vorticity is produced along the body surface and shed into the wake and to understand how this rules the behavior of the vortical force and torque.

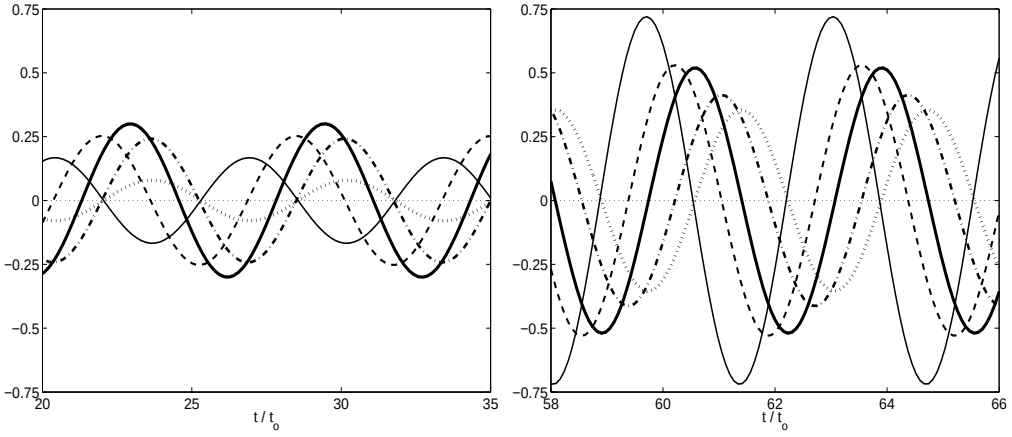

Figure 8. Time evolution of F^y_{ur} (– –), F^y_g (–·–), F^y_ω (—), Γ^z_ω (···) and v (−); θ is superimposed to F^y_g; On the left : thick body with $\chi = 3$, $Re = 180$, $St = 0.125$ and $\overline{u} = 1.23$; On the right : thin body with $\chi = 10$, $Re = 240$, $St = 0.275$ and $\overline{u} = 1.17$.

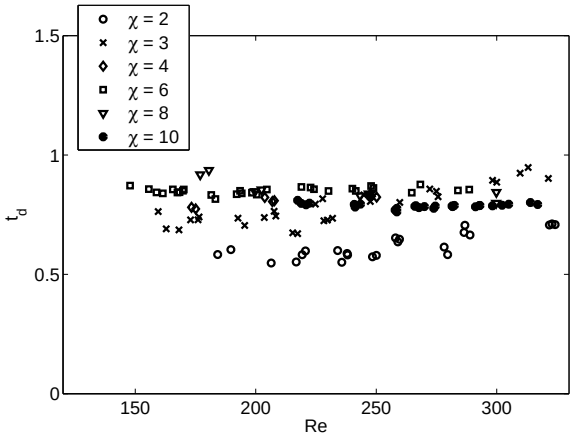

Figure 9. Dimensionless time delay between the oscillation of the transverse vortical force and that of the vortical torque as a function of Re and χ.

Acknowledgements

We are very grateful to D. Fabre, H. Ayroles, S. Cazin, E. Cid, C. Trupin, J.-P. Escafit, J.-J. Huc and O. Eiff for technical assistance and helpful discussions.

References

[1] A. Andersen, U. Pesavento, and Z.J. Wang. Unsteady aerodynamics of fluttering and tumbling plates. *J. Fluid. Mech.*, 541:65–90, 2005.

[2] C. Brücker. Structure and dynamics of the wake of bubbles and its relevance for bubble interaction. *Phys. Fluids*, 11:1781–1796, 1999.

[3] K. Ellingsen and F. Risso. On the rise of an ellipsoidal bubble in water: oscillatory paths and liquid - induced velocity. *J. Fluid. Mech.*, 440:235–268, 2001.

[4] P. Ern, P.C. Fernandes, F. Risso, and J. Magnaudet. Evolution of wake structure and wake-induced loads along the path of freely rising axisymmetric bodies. *Phys. Fluids*, under consideration, 2007.

[5] P.C. Fernandes, P. Ern, F. Risso, and J. Magnaudet. On the zigzag dynamics of freely moving axisymmetric bodies. *Phys. Fluids*, 17:098107, 2005.

[6] P.C. Fernandes, P. Ern, F. Risso, and J. Magnaudet. Dynamics of axisymmetric bodies rising along a zigzag path. *J. Fluid Mech.*, under consideration, 2007.

[7] P.C. Fernandes, F. Risso, P. Ern, and J. Magnaudet. Oscillatory motion and wake instability of freely-rising axisymmetric bodies. *J. Fluid Mech.*, 573:479–502, 2007.

[8] S. Field, M. Klaus, M. Moore, and F. Nori. Chaotic dynamics of falling disks. *Nature*, 388:252–254, 1997.

[9] M. Howe. On the force and moment on a body in an incompressible fluid, with application to rigid bodies and bubbles at low and high Reynolds numbers. *Q. J. Mech. Appl. Math.*, 48:401–426, 1995.

[10] M. Jenny, J. Dusek, and G. Bouchet. Instabilities and transition of a sphere falling or ascending in a newtonian fluid. *J. Fluid. Mech.*, 508:201–239, 2004.

[11] M.A. Jones and M.J. Shelley. Falling cards. *J. Fluid. Mech.*, 540:393 – 425, 2005.

[12] P. Kry and R. List. Angular motions of freely falling spheroidal hailstone models. *Phys. Fluids*, 17(6):1093–1102, 1974.

[13] H. J. Lugt. Autorotation. *Ann. Rev. Fluid. Mech.*, 15:123–147, 1983.

[14] J. Magnaudet and I. Eames. The motion of high-Reynolds-number bubbles in inhomogeneous flows. *Ann. Rev. Fluid Mech.*, 32:659–708, 2000.

[15] G. Mougin and J. Magnaudet. The generalized Kirchhoff equations and their application to the interaction between a rigid body and an arbitrary time-dependent viscous flow. *Int. J. Multiphase Flow*, 28:1837–1851, 2002.

[16] G. Mougin and J. Magnaudet. Path instability of a rising bubble. *Phys. Rev. Lett.*, 88(1):14502, 2002.

[17] G. Mougin and J. Magnaudet. Wake-induced forces and torques on a zigzagging/spiralling bubble. *J. Fluid Mech.*, 567:185–194, 2006.

[18] W. Shew, S. Poncet, and J.-F. Pinton. Force measurements on rising bubbles. *J. Fluid Mech.*, 569:51–60, 2006.

[19] G. E. Stringham, D. B. Simons, and H. P. Guy. The behavior of large particles falling in quiescent liquids. *US Geol. Surv. Prof. Pap.*, 562-C:C1–C36, 1969.

[20] Z.J. Wang. Dissecting insect flight. *Ann. Rev. Fluid Mech.*, 37:183–210, 2005.

[21] W. Willmarth, N. Hawk, and R. Harvey. Steady and unsteady motions and wakes of freely falling disks. *Phys. Fluids*, 7(2):197–208, 1964.